Modularized, Reconfigurable and Bidirectional Charging Infrastructure for Electric Vehicles with Silicon Carbide Power Electronics (MoReSiC)

Deliverable D.5.2 (Month 27)

Title: "Laboratory prototype of the non-isolated DC/DC converter."

Authors:
Radosław Sobieski, Markel,
Rafał Kopacz, Warsaw University of Technology.

NTNU
Norwegian University of Science and Technology

Iceland Liechtenstein Norway eea grants norway grants

Warsaw University of Technology

Executive summary

The deliverable includes the developed, built, and tested non-isolated DC/DC converter operating as the battery interface in the MoReSiC system. Furthermore, it includes additional studies on the proposed common-leg coupled inductor configuration for the system. The deliverable was performed by the joint work Markel employees and Warsaw University of Technology team.

After the prior analysis from D.5.1, supplying the converter control algorithm capable of operation in all modes and with supplementary DC link (+/-750V) voltage balancing, a final experimental model has been designed and constructed.

The three-level synchronous topology was selected, and the submodule developed in the frame of WP2 was included as the base for the DC/DC converter. At first, a series of simulations were performed in PLECS to analyze the possible inductor configurations and the different modulation strategies, as well as their impact on the rest of the converters. Furthermore, control loops for both DC-link voltage balancing and inductor current leveling were developed. Then, two prototypes were constructed and validated in experimental tests.

Table of Contents

1. Topology selection for the non-isolated DC/DC converter

The research in WP5 started with the selection of a proper topology for the non-isolated DC/DC battery converter under the first task: T5.1 *Assessment of the fundamental design of a non-isolated DC/DC converter topology enabling bidirectional operation and three-level voltage on the high side*. The critical function of this power electronics system is to interface the power flow from the three-wire DC-link (+750/0/-750 V) in the charging station and the battery energy storage system rated at 800 V nominal voltage, assuming the energy flow in both directions (from and to the battery energy storage). Furthermore, it is required that the converter is capable of balancing the voltages of the three-wire DC-link in case of operation without the AC/DC converter being turned on. Finally, since the converter was developed in the frame of the MoReSiC system, the converter had to be designed using 1.2 kV SiC power devices, and the three-level power submodules developed within the other part of the project (WP2).

On the basis of prior work in other work packages, especially WP3, some potentially prominent topologies, such as the Flying Capacitor Converter (FCC) and T-type converter, were decisively dismissed as in these topologies, there is no connection to the 0 V potential in the three-wire DC-link structure, thus, making it impossible to balance the voltage between the DC-link capacitors. Furthermore, it is derivative of the ANPC topology chosen for the grid converter, and only using four transistors per leg, a well-known three-level DC/DC converter structure, also referred as double synchronous converter, can be established, as shown on the example of a single leg in Fig. 1. This topology is very straightforward, has a low component count and is capable of reaching high efficiencies, as well as meets all the requirements sourced in the MoReSiC system and described above. To be more thorough, in order to use the ANPC submodules, only a minor change has to be made – the additional two transistors have to be omitted, and two paths have to be shorted. Thus, the submodule can be easily used in this system without any changes to the PCB scheme established before.

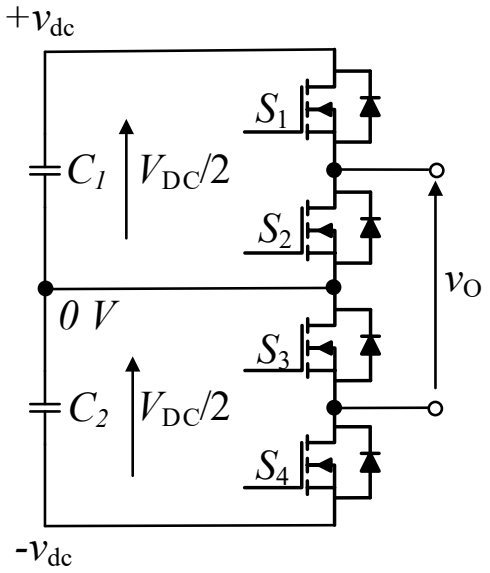

Fig. 1 Single leg of the three-level DC/DC converter.

However, to meet the expected power rating (20 kW) and fully comply with the rest of the charging system, most importantly with the submodule from WP2 capable of transferring maximally 10 kW, at least two submodule units had to be employed. Furthermore, lowering the output ripples of the converter is especially important for battery-oriented systems, as in this case. Thus, an interleaved structure is recommended. Here, a two-phase system is initially chosen, as for the considered battery system with 800 V nominal voltage, operating points near D=0.5 result in the lowest ripples (DC supply at 1500 V).

The whole DC/DC converter in the chosen three-level topology, on the example of a buck configuration, is depicted in Fig. 2. Here, apart from the two legs built from the submodules, an output capacitor for lowering the output voltage ripples has to be added, along with a group of inductors, here shown in the most straightforward configuration (four non-coupled inductors).

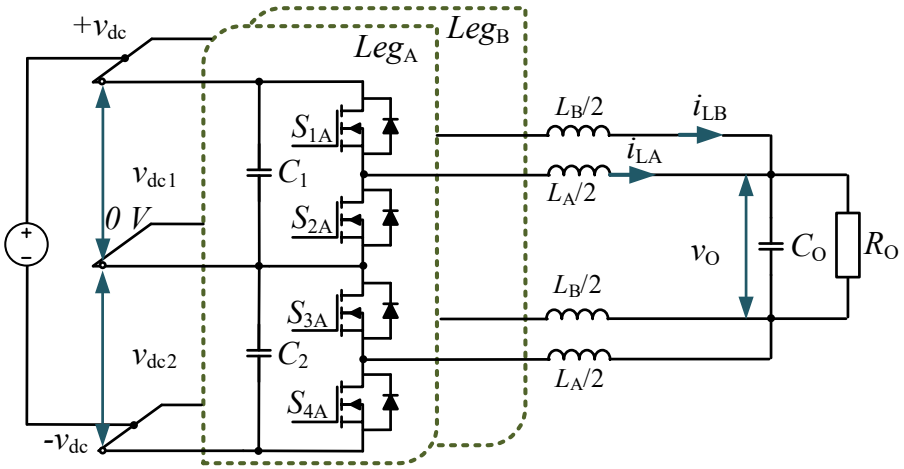

Fig. 2 The chosen topology of the DC/DC converter with four single inductors (in exemplary buck configuration).

2. Inductor configurations, modulation strategies & control

While the basic topology of the three-level DC/DC converter is straightforward in terms of the leg structure, the possible modulation strategies and the different applicable inductor configurations render the system more complex. Considering these options is essential to establish an optimized system for a specific application, such as a non-isolated DC/DC converter operating as a battery interface in a bipolar fast charging station system, and preparing the control scheme. This section is directly associated with task T5.2 *Theoretical and simulation-based verification of various configurations of the non-isolated DC/DC converters for supplying charging power in the range of 10-20 kW,* as the theoretical analysis is considered here, while the simulation verification is described in the next section.

At first, the possible inductor configurations were analyzed. Based on a thorough literature review, prior experiences of the team, and new ideas, four possible solutions were found, as shown in Fig. 3. The first approach, depicted in Fig. 3a, is the most conventional – to use four separate non-coupled inductors (SI). This method is very straightforward. The construction of the magnetic components is the simplest, and in accordance with the analysis described in the next section, all modulation strategies are applicable. However, since four single inductors are used, the volume of the magnetics is notable, specifically when compared to other more sophisticated solutions with coupled inductors.

Using coupled inductors is a well-known technique to limit the total volume, as instead of using four magnetic cores, only 2 are required. Furthermore, with proper orientation of the flux within the magnetics, the inductor ripples can also be minimized. Here, two possible configurations were found. Fig. 2b presents the state-of-the-art topology from the literature, with two common-potential coupled inductors, hereby named the tapped inductor approach (TI). In this configuration, the coupled inductor is connected based on the potential of the converter legs – in one inductor, it is the positive potential (terminal A+ and B+), and in the other, the negative one (A-, B-). In such a situation, when negative coupling is used, the output ripples, especially important for battery-oriented applications, are lowered compared to the conventional solution (SI). Here, all modulation schemes are also possible. The option shown in Fig. 3c, the four-winding coupled inductor (4WI), is a variation of the TI approach, where the coupled inductors are enclosed in one core. However, given the limitations in the very low coupling coefficient required, the TI and 4WI options are nearly identical in terms of performance and design.

The final configuration also employs coupled inductors. However, in this case, the connection is different, as shown in Fig. 3d. The coupled inductors are connected in a common-leg configuration (2CI), one inductor to terminals A+. A-, and the other to B+. B-. When a positive coupling is applied, this configuration also shows low output ripples, especially for duty near 0.5, which is the case of the battery DC/DC converter in the MoReSiC system. However, this configuration cannot be controlled with all the modulation strategies, which is elaborated on further in this report. Moreover, this idea is novel and has been proposed in the scope of the project.

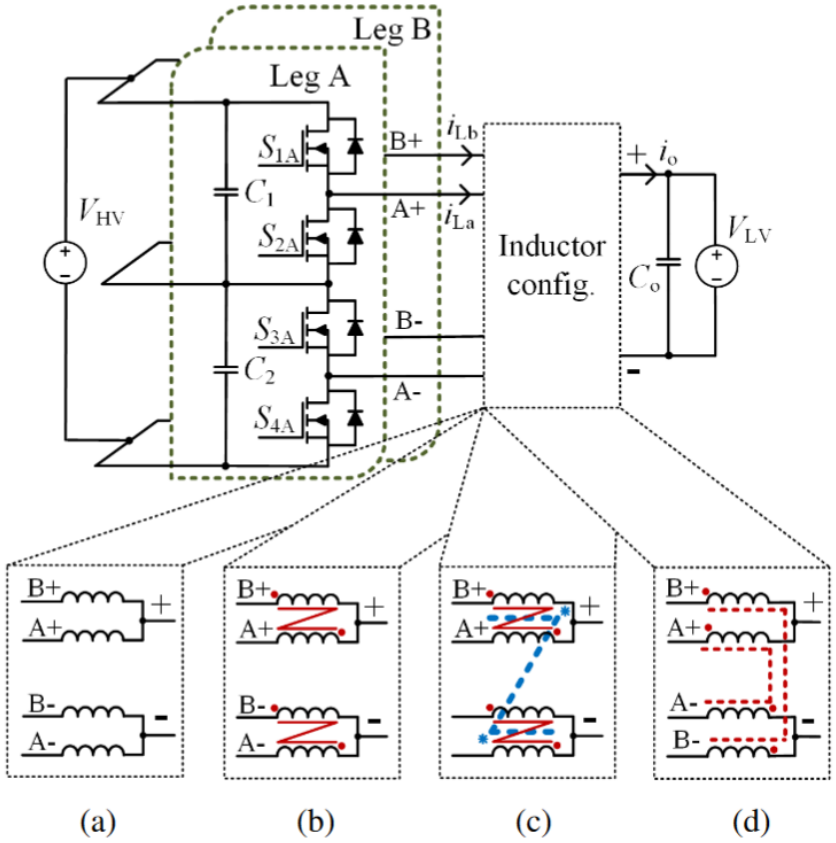

Fig. 3 Possible inductor configurations for the DC/DC converter: (a) four single inductors (SI), (b) two tapped inductors (TI), (c) four-winding coupled inductor (4WI), (d) common-leg coupled inductor (CI). Options a)-c) are state-of-the-art solutions, whereas option d) has been proposed by MoReSiC participants.

Another crucial consideration regards the modulation technique. In the DC/DC converter of interest, four main modulation strategies can be named and are shown in Fig. 4. The first modulation, depicted in Fig. 4a, is the conventional non-interleaving modulation (referred to as I-type), where the two legs are controlled with the same signals. Using this scheme, the system actually becomes equal to a single-phase non-interleaved system, and even a single inductor (with an inductance equal to 4 times the inductance of each of the four separate inductors) can be used. Generally, the multi-phase character of the system is not utilized in this modulation method, and thus the ripples are quite high. However, since the DC/DC converter has to be made employing at least two submodules (2 x 10 kW), it can still be applied. Furthermore, using this strategy, no current balancing techniques need to be employed, as natural current balancing occurs.

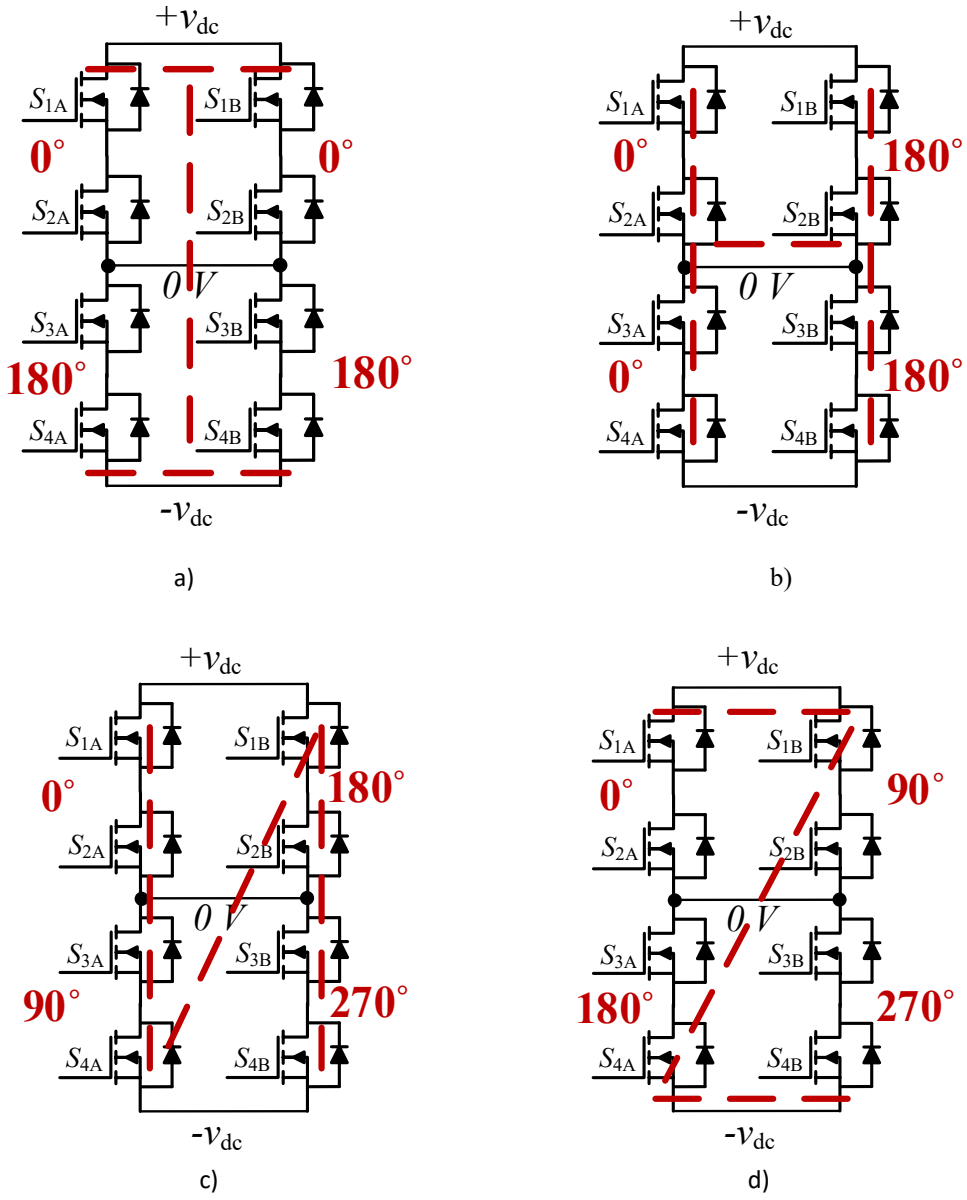

Fig. 4 Modulation strategies applicable in the DC/DC converter: a) conventional non-interleaving modulation (I), b) conventional interleaving modulation (H), c) N-type interleaving modulation (N), d) Z-type interleaving modulation (Z).

The second modulation technique, shown in Fig. 4b, is the conventional interleaving modulation (here referred to as H-type). In this method, the two legs are shifted in phase by 180 degrees. Thus, the inductor currents cancel out, and the output ripples are minimized. This is the technique that can be effectively used in the 2CI configuration. The third modulation strategy is the N-type technique. Similarly, as for the other modulations, the name refers to the phase shifts in the transistor control signals, as depicted in Fig. 4c. Applying this technique makes the output ripples even lower, however, with a slight cost in the form of additional power losses. Finally, the Z-type technique presented in Fig. 4d is similar to the N-type in terms of output ripples. However, it is usually considered inferior to the N-type in the literature, as it shows higher EMI.

Exemplary transistor control signals for the most complex strategy, the N-type modulation, with the expected inductor currents, along with the description of the basic switching states of the converter, are shown in Fig. 5 and Tab. 1, respectively.

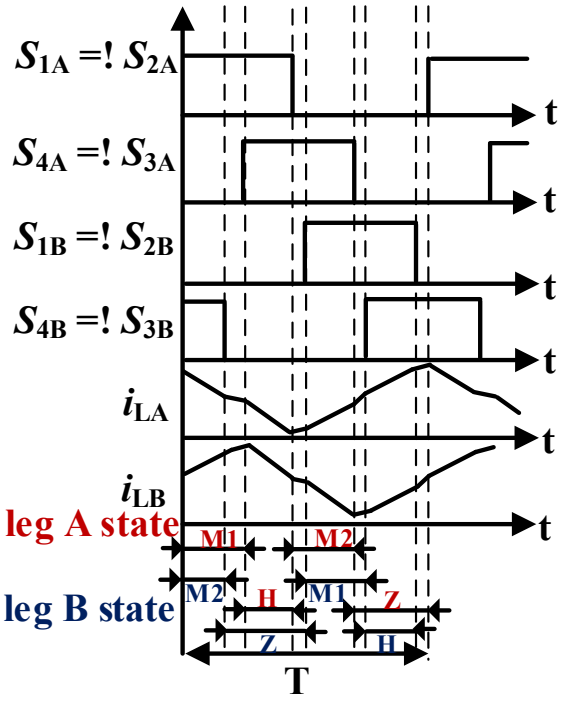

Fig. 5 Exemplary transistor control signal for the N-type modulation strategy.

Tab. I Basic switching states of the DC/DC converter in buck mode

State	S_1	S_2	S_3	S_4	Output voltage
High state (H)	1	0	0	1	V_{DC}
Medium state 1 (M1)	1	0	1	0	$V_{DC}/2$
Medium state 2 (M2)	0	1	0	1	$V_{DC}/2$
Zero state (Z)	0	1	1	0	0

Considering all the possible modulation strategies, along with the different inductor configurations, a control scheme was prepared for each of the methods. Thus, the many options could have been compared, both in simulations and later on in the experimental prototype. The proposed control system is shown in Fig. 6 on the example of buck mode operation. This converter with the control system is also applicable in boost mode with the opposite direction of power flow, as long as the voltage controller is driven by the grid-side DC voltage values, depicted as V_{dc}. Furthermore, in Fig. 6, the SI configuration is presented. Note that the method is nearly identical for all configurations and modulation techniques.

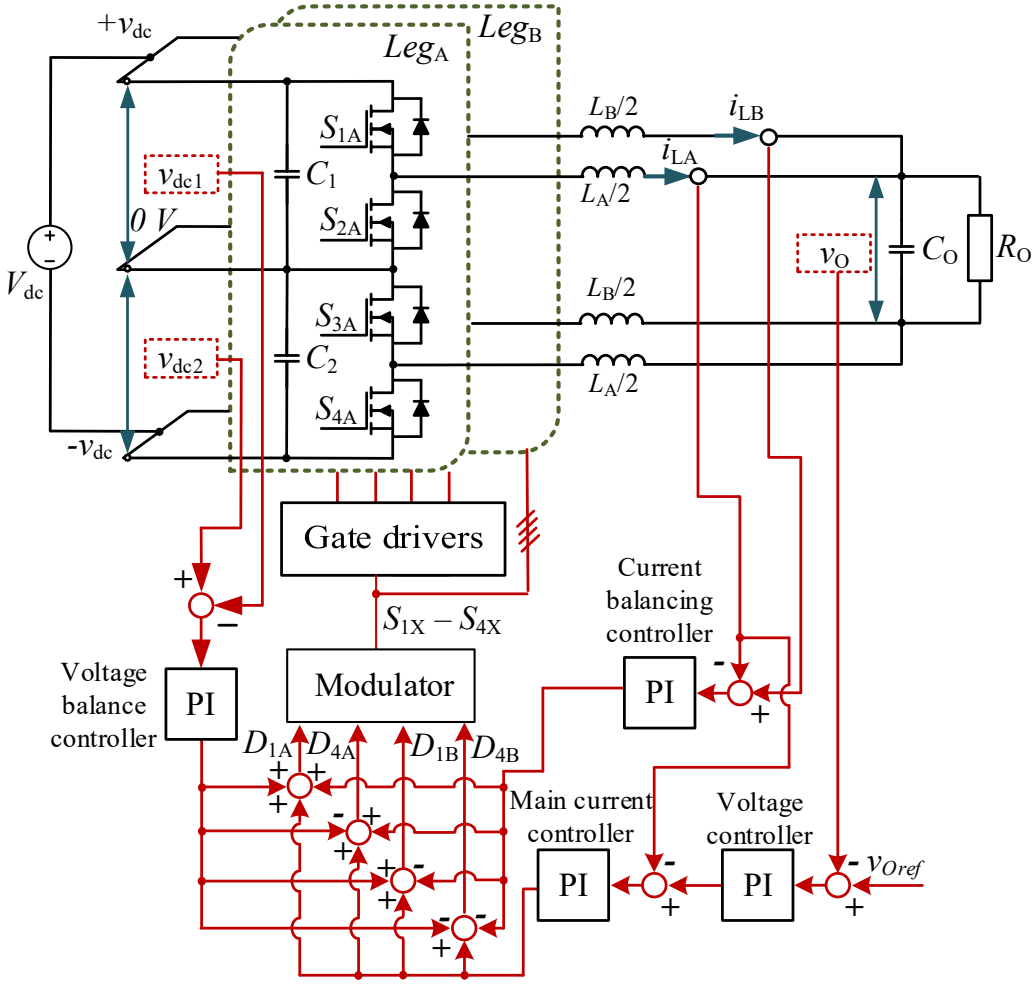

Fig. 6 Control scheme for the DC/DC converter, shown in the example of buck mode operation.

In the system, the core control path consists of a primary current PI (proportional-integral) controller and a secondary voltage controller, where the reference value of the output voltage is given. Using the output of the main current control, the dominant part of duty cycles D_A (for leg A) and D_B (for leg B) are calculated and used to drive the converter.

However, additional balancing measures are required for the proper operation of the converter. Firstly, the 3-pole DC bus connection necessitates leveling the DC voltages at capacitors C_1 and C_2. Based on an error value from the difference between the measured v_{dc1} and v_{dc2} voltages, a voltage-balancing PI controller regulates the duty cycles of the converter. The output of the controller is either added (for signal S4=!S3) or subtracted (in the case of signal S1=!S2) to the duty cycle value. Therefore, such an approach allows for voltage balancing without affecting the output voltage.

Furthermore, balancing currents between the interleaved legs is also a necessity in most modulation techniques to limit the currents circulating in the inductors and minimize additional power losses. This can be achieved through two separate control paths consisting of a voltage and a current controller for each leg. However, using this method, the total count of controllers is five. Thus, in the presented system, another approach was assumed to limit the number of regulators. The core control path (voltage and main current controllers) is used to set the duty cycles for both legs, and an additional current controller using the difference between the inductor currents i_{LA} and i_{LB} as an error is used. Therefore, the output from the current balancing

controller is added to the D_A value and subtracted from D_B, and similarly, as in the voltage balancing controller, the output is unaffected. Moreover, apart from lowering the number of total regulators to four, the current balancing controller is less susceptible to noise, as the error uses two measured values as an input, and therefore, the interferences cancel out.

All in all, the proposed control diagram fulfills all requirements issued by the MoReSiC charging system, including voltage and current balancing, as well as bidirectional operation, and could have been used in further analyses, both in simulations and experiments, as well as in the final converter (deliverable D.5.2). Thus, task T5.3 *Development of the DC/DC converter control algorithm including DC voltage balancing system and operation at maximum efficiency in different operation modes* was completed.

3. Simulation study

The next step was to develop simulation models and perform the simulation study to finish tasks T5.2 *Theoretical and simulation-based verification of various configurations of the non-isolated DC/DC converters for supplying charging power in the range of 10-20 kW,* and also T5.4 *Identification of electrical and thermal operating parameters in terms of voltage, current and temperature.* Similarly, as in the other work packages, PLECS software from Plexim was used, as it provides the possibility to simulate both the control and operation of the converter, as well as to help with the power loss estimation required for the identification of the electrical and thermal operating parameters for the design of the experimental model, both for WP2 and WP5.

The results from the exemplary simulation performed in the steady state are showcased in Fig. 7 and 8. Please note that only results for inductor configuration SI and N-type modulation are shown here, while other configurations were also tested. The results from the study at the nominal operating point at 1500 V input, 800 V output, and 20 kW power is depicted in Fig. 7, while another point, directly correlating with the exemplary experimental test shown further in the report, performed at 800 V input, 590 V output, and power of 10 kW is shown in Fig. 8. As can be observed, the control system operates as assumed: the output voltage is steady at the reference value, the DC bus voltages are well-balanced with minimal ripples, and the inductor currents are leveled as well. Moreover, even though the momentary currents of individual inductors are high due to the interleaved structure and N-type modulation, the ripple of the sum inductor current is at low levels, at roughly 5% of the nominal value. Therefore, ripples of both output current and voltage are minuscule. However, it is worth noting that in a real-life application, the connections, e.g., cables, to the battery energy storage system can be lengthy, and thus, extra parasitic inductance appears, causing the output ripples to increase radically. Moreover, it can be seen that using the N-type modulation, the current shape is either triangular (for duty near 0.5) or closer to a trapezoidal shape. All in all, the simulations prove that the DC/DC converter can adequately operate with the presented control system.

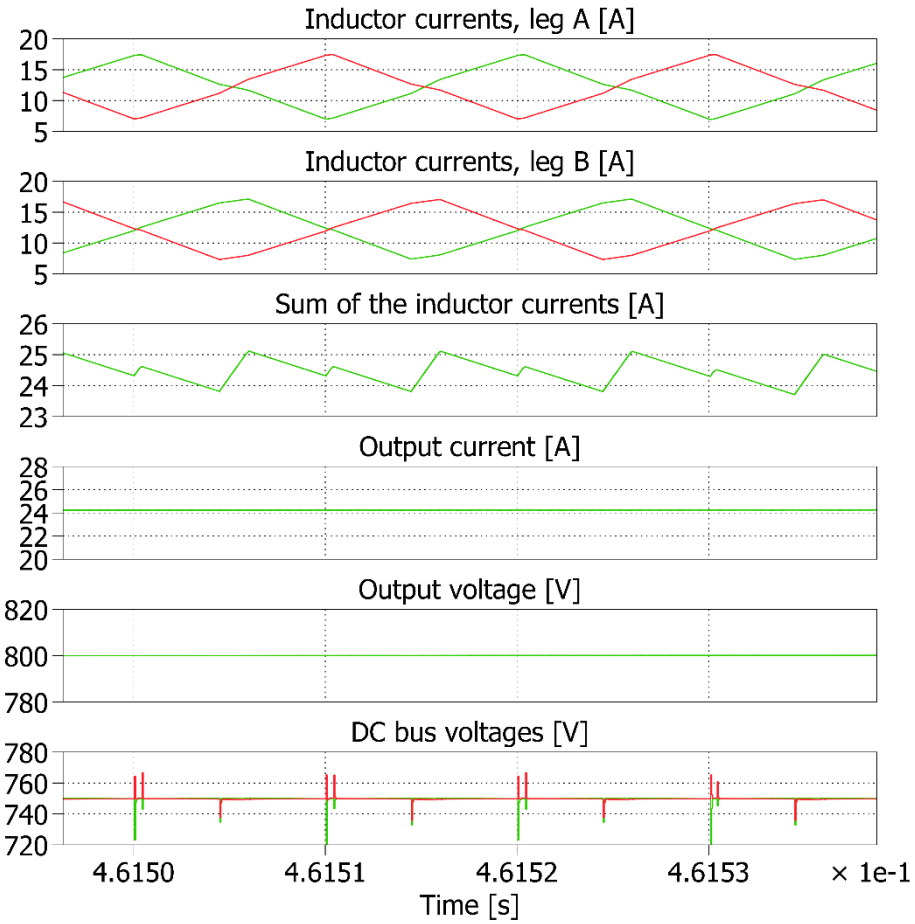

Fig. 7 Exemplary simulation results of the DC/DC converter – case 1, 1500 V input, 800 V output, 20 kW power.

Finally, the last part of the simulation study regarded the establishment of the electrical and thermal operating parameters for the design of the experimental model. Thus, a power loss-oriented study was conducted for different types of transistors and the number of interleaved legs (2 or 3). Based on the results from this research (depicted in Fig. 9, and a similar study made for the grid converter, the NTH4L040N120SC1 transistor was chosen as the most efficient one compared to other state-of-the-art and available 1200 V-rated SiC MOSFETs, thus completing task T5.4 *Identification of electrical and thermal operating parameters in terms of voltage, current and temperature.*

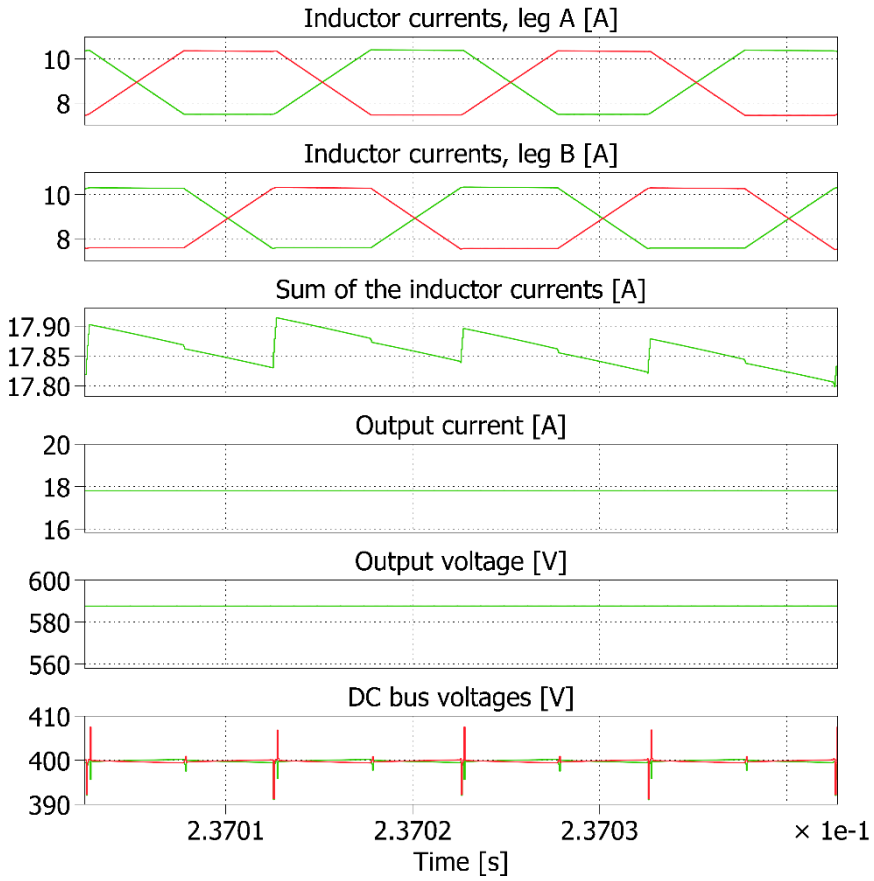

Fig. 8 Exemplary Simulation results of the DC/DC converter – case 2, 800 V input, 590 V output, 10 kW power..

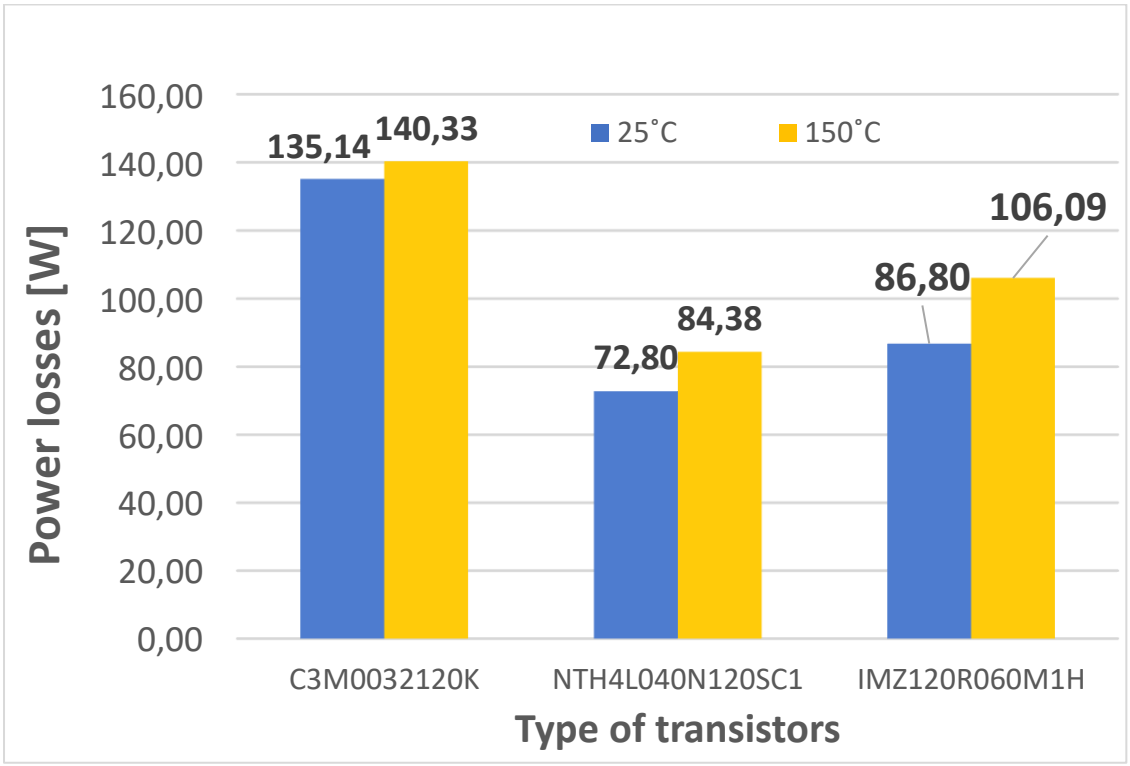

Fig. 9 Simulation-based assessment of power losses for different state-of-the-art SiC MOSFETs.

4. Initial experimental prototype of the converter

In order to validate the control scheme of the DC/DC converter, an early experimental prototype was designed and constructed. Thus, work on task T5.5 *Design of the non-isolated DC/DC converter including main circuit layout with the necessary auxiliary sub-circuits and high-frequency magnetic components* has already started. To expedite the process, an available control board constructed earlier in other projects at WUT was used. Moreover, because of the problems with the availability of the components, also the measurement circuits for the voltages and currents were based on systems developed for other converters. While these solutions were not ideal for the DC/DC battery converter, they were sufficient to test the control method and validate it, while the final version would have a dedicated system, both for the DSP control as well as the measurement and conditioning systems.

The basic parameters of the early prototype of the DC/DC converter are the same as those for the final version and are presented in Tab. II. The DC-link voltage is 1500 V (750 + 750), while the nominal output (battery) voltage is 800 V. In order to limit the power losses and omit potential issues in communicating the DC/DC converter with the grid ANPC converter, the frequency was set to 62.5 kHz. Furthermore, the inductor values were calculated as roughly 620 µH total, with 60 µF output capacitance to reach output ripples below 2%. Please note that four inductors in SI configuration are shown in the prototype as the basic, conventional solution. However, other configurations have also been tested with different inductors connected and other modulations applied. Finally, the system uses two power submodules from WP2, shown in Fig. 10, with four transistors per each leg.

Tab. II Basic parameters of the 20 kW DC/DC converter

Nominal battery voltage	800 V
DC-link voltage $V_{dc1} + V_{dc2}$	1.5 kV
Switching frequency	62.5 kHz
Filter inductances L_A, L_B, L_C	4 x 155 µH
Battery-side capacitance	60 µF
DC-link capacitances	4 x 60 µF
Power SiC transistors	8 x NTH4L040N120SC1
Number of submodules (WP2)	2

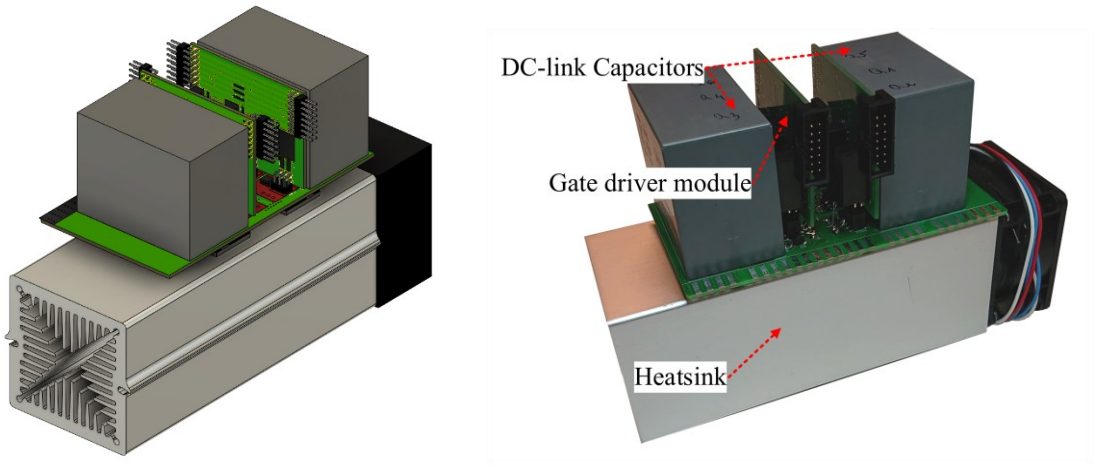

a) b)

Fig. 10 The power submodule (WP2): a) 3D model, b) photo.

Apart from the power circuit, two submodules, and the inductors, the system was built using a control board based on TMS320f28379D digital signal processor and a number of measurement circuits. Except for the core ones enumerated in the control section (two DC bus voltage measurements, output voltage measurement, and two inductor current meters), more measurements are required for the full charging station operation. To be more specific, the power flow into and out of the converter must be measured. Thus, an additional output current meter and two input current measurements were added (one per half of the DC bus). All the current meters were constructed using LEM transducers, LA-55 for the inductor currents and LAH-50 for the DC currents. The voltage measurements were based on self-made PCBs, using optocouplers and amplifiers to construct an isolated voltmeter system.

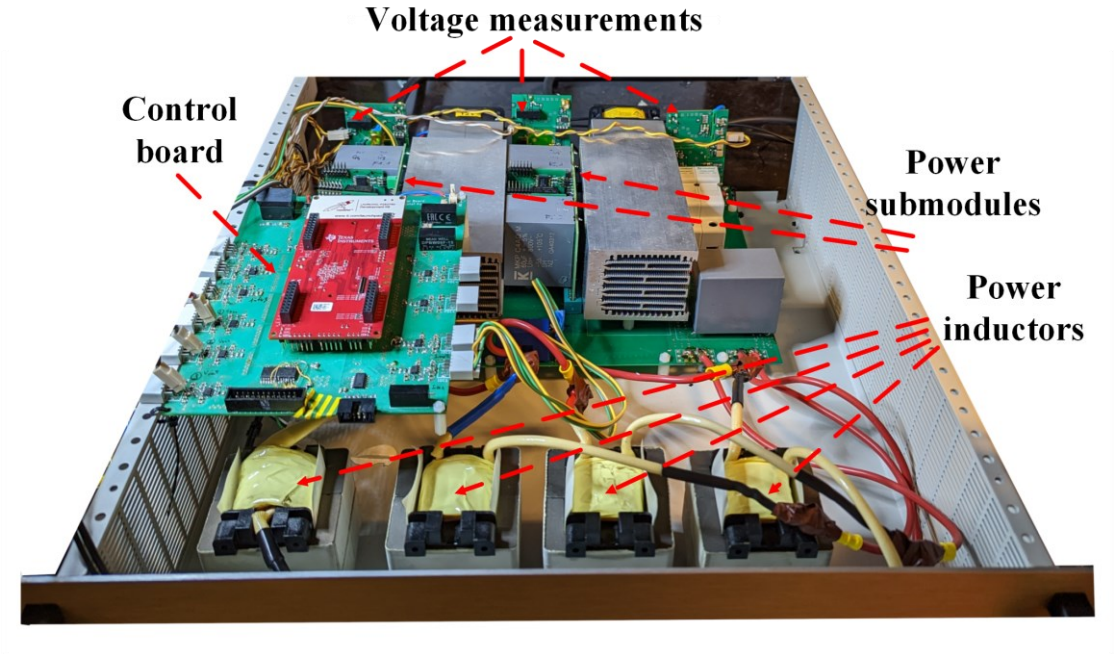

Fig. 11 Photo of the initial experimental prototype constructed for validation of the control algorithm.

5. *Final experimental prototype of the converter*

Despite the initial prototype being operational, a second, final experimental model has been developed to improve the design and flesh out some minor issues, mainly related to noise issues in the control and measurement part. More specifically, the control board, measurement, and conditioning systems have been re-designed so that full communication with the station was assured, excess EMI noise was minimized, and full operation capability was reached. The photograph of the second prototype is depicted in Fig. 12.

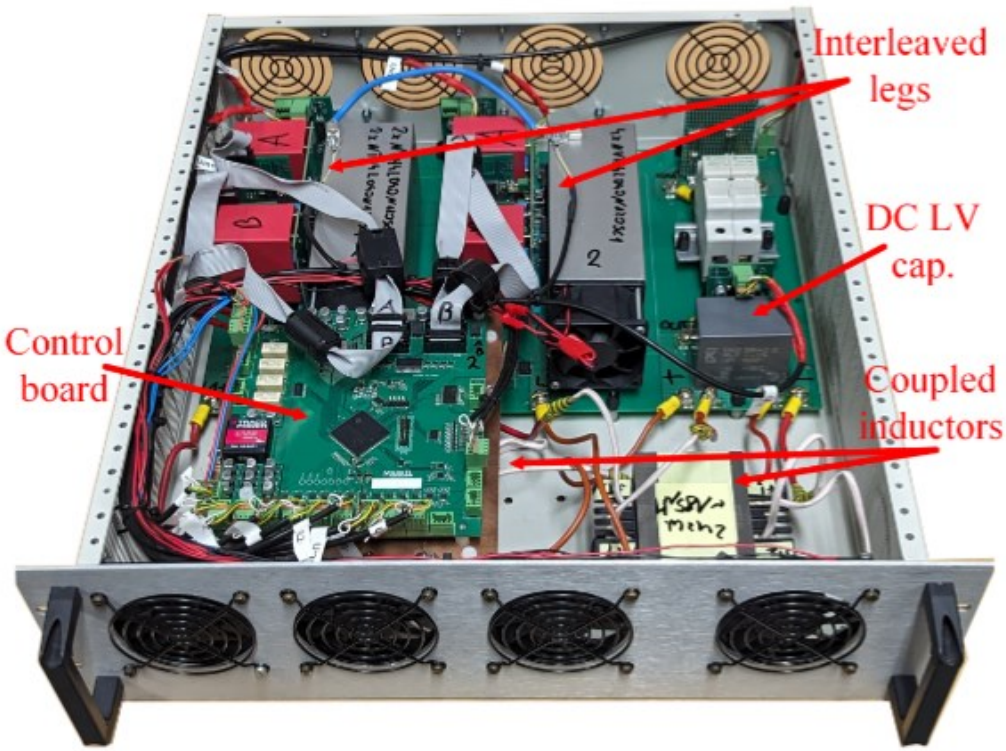

Fig. 12 Photograph of the final experimental prototype. The photo has been taken with the inductors in CI configuration.

The core power circuit parts, e.g., the submodules, power boards, and inductors, are identical in both experimental models. However, as stated above, the control & measurement part has been designed anew to fully comply with the requirements and project assumptions. Thus, the new control board was highly reminiscent of the design employed for other converters in the system and was based on the TMS320f28388D digital signal processor, with several conditioning circuits in single-ended and differential configuration to optimize the measurement loops, as well as CAN interface integration, to communicate with the rest of the system. Furthermore, the voltage measurements (2 DC-link ones and one on the battery side) were constructed with AMC1411 ICs from Texas Instruments to support high-bandwidth operation with limited noise compared to the prior solution. Similarly, the inductor current measurements were also changed to allow for a more accurate representation of high-frequency currents; these were constructed with MCA1101 ICs from Aceinna. Thus, this hardware implementation allowed for the full required capabilities of the converter, and task T5.5 *Design*

of the non-isolated DC/DC converter including main circuit layout with the necessary auxiliary sub-circuits and high-frequency magnetic components has been completed.

6. Hardware validation of the final converter prototype

Using the built final converter experimental model, a series of experimental tests showcasing the proper operation of the converter under the proposed control system were performed. The results from the experiments are presented in Fig. 13 and 14, and depict the operation of the converter at 20 kW of power, 1200 V DC-link voltage, and 600 V of voltage at battery-side, for the both directions of operation (Fig. 13 – power drawn from the storage, Fig. 14 – power delivered to the storage). Analyzing the Figures , it can be seen that the DC-link voltages are decently leveled using the presented voltage balancing method, with a difference below 2% of the nominal DC voltage (roughly 14 V) and some minor overshoots appearing at the time of transistor switching (at approximately 40 V). Therefore, the voltage among the transistors in the multilevel structure is balanced as well, providing safe operating conditions for the converter. Furthermore, the output current of the converter is characterized by very low ripples below 1 A, corresponding to less than 5% of the I_{BAT} steady-state value. This is crucial since the converter is designed to cooperate with a battery energy storage system. Finally, the output voltage is stable and reaches the reference value of 600 V.

Thus, task T5.6 *Delivery and initial tests of the non-isolated DC/DC converter in all operation modes* has been finished.

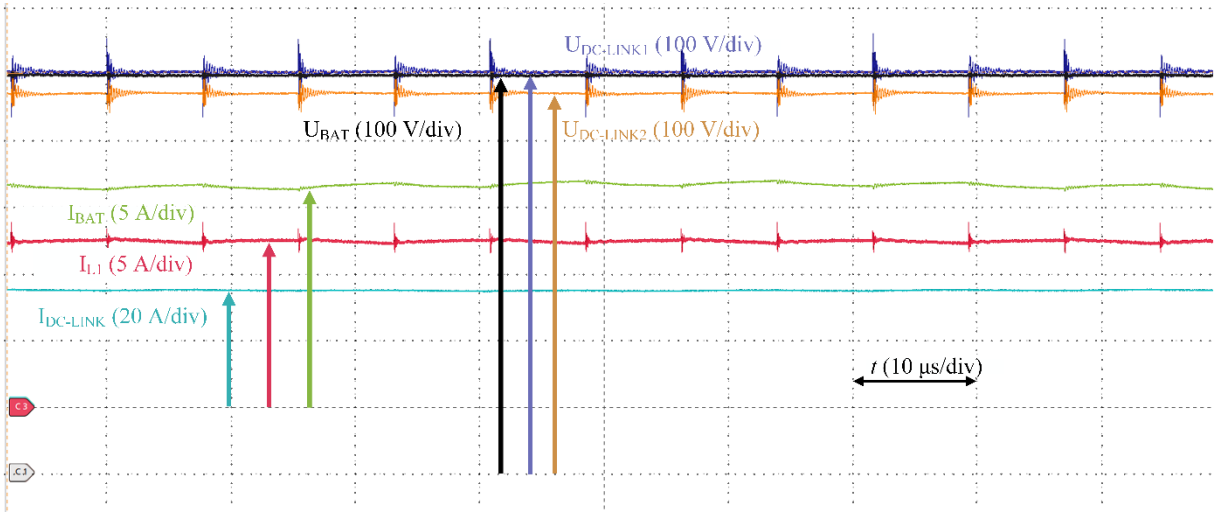

Fig. 13 Exemplary results at full power of 20 kW, power drawn from the storage.

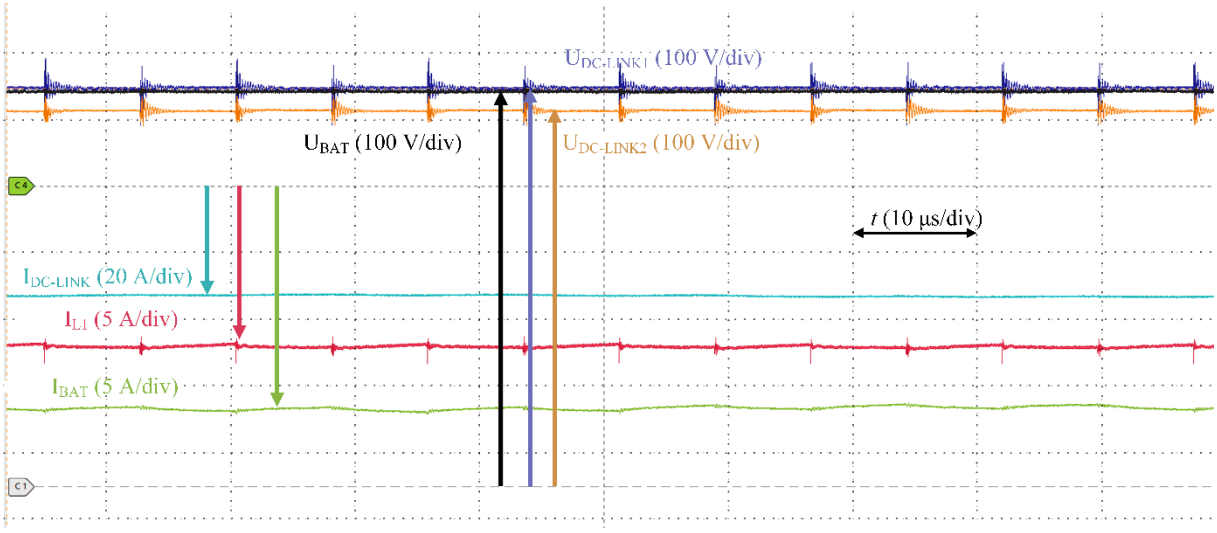

Fig. 14 Exemplary results at full power of 20 kW, power delivered to the storage.

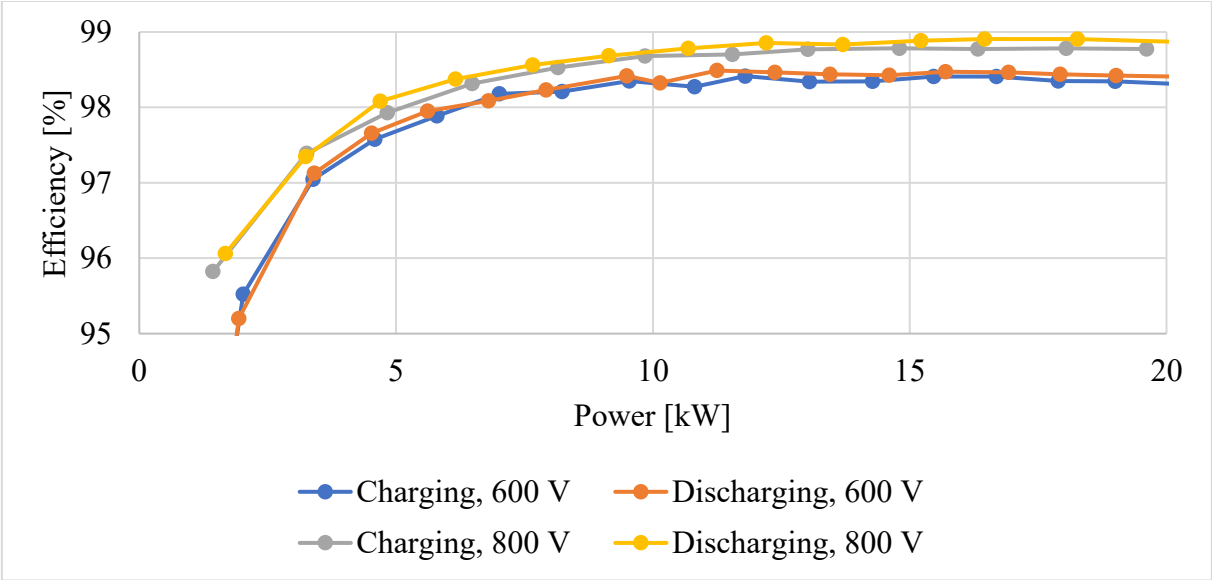

Fig. 15 Efficiency characteristics for up to 20 kW of power, in both directions of power flow, with the battery side voltage at 600 and 800 V.

In fact, it has been validated that the designed and constructed DC/DC converter prototype under the developed control method behaves as anticipated, with balanced DC-link voltages and inductor currents, and low output ripples. Thus, it can be effectively applied in a bipolar grid-based EV charging station in WP6.

7. Proposed common-leg coupled inductor configuration

The model has also been employed to study the proposed novel common-leg configuration. Exemplary operation of the converter with the suggested structure with H-type modulation is depicted in Fig. 16. As can be seen, when H-type modulation is employed, the inductor current ripple frequency is equal to the switching frequency and is shifted by 180°. That results in the

output current frequency being two times higher than the switching frequency. Moreover, the important difference between the considered control technique and other state-of-the-art methods is that the common-mode voltage is zero in the proposed solution. Fig. 17 shows a comparison of inductor and output current ripples for the proposed and other control methods.

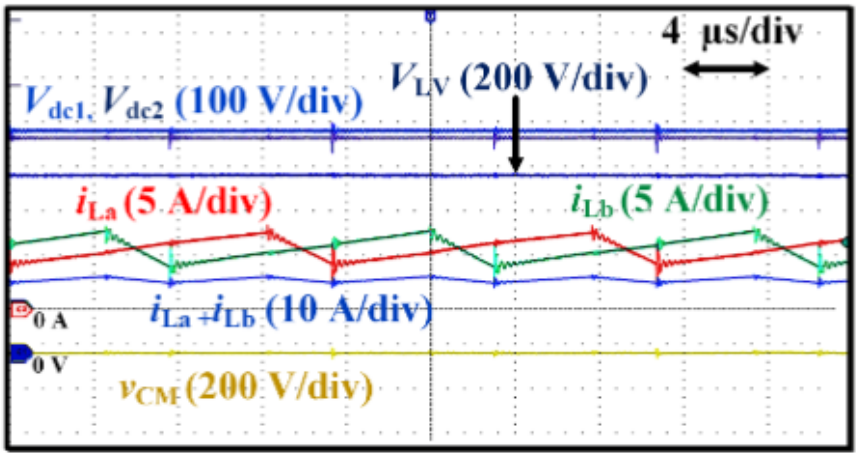

Fig. 16 Exemplary experimental results for the H-type modulation in CI configuration performed at 1 kV DC, 10 kW of power, and G_V=0.8.

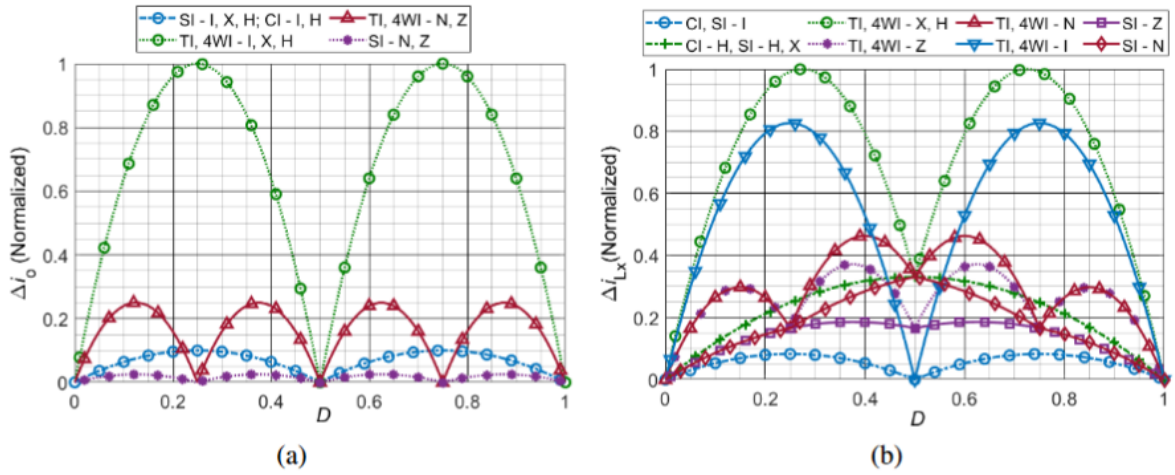

Fig. 17 Current ripples comparison for different inductor configurations and modulation strategies: (a) output current ripples, (b) inductor current ripple.

Further, Fig. 18 exhibits the efficiency characteristics for the proposed (CI) and the conventional approach (SI). As shown, the efficiency remains at a high level for the two analyzed inductor configurations, indicating that the use of two coupled inductors (CI) instead of four individual inductors (SI) has a positive but modest impact on efficiency. Finally, Fig. 19 depicts the experimental comparison of generated common-mode (CM) voltage. The CM voltage level for the proposed solution is significantly lower; for example, at a switching frequency equal to 62.5 kHz and doubled switching frequency, the CM voltage level in H-type modulation is lower by 8.1 dB and 47.5 dB, respectively. In the proposed method, utilizing the H-type control strategy, CM noise is almost completely eliminated. Consequently, the CM filter

can be omitted, or at least substantially reduced, providing a substantial positive impact on the power density of the converter.

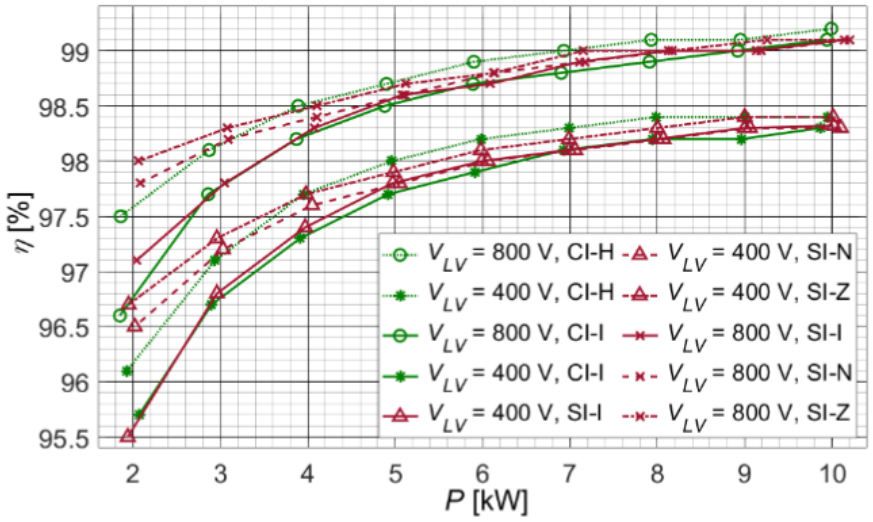

Fig. 18 Efficiency characteristics comparing the proposed CI solution and the conventional SI approach for various modulation methods.

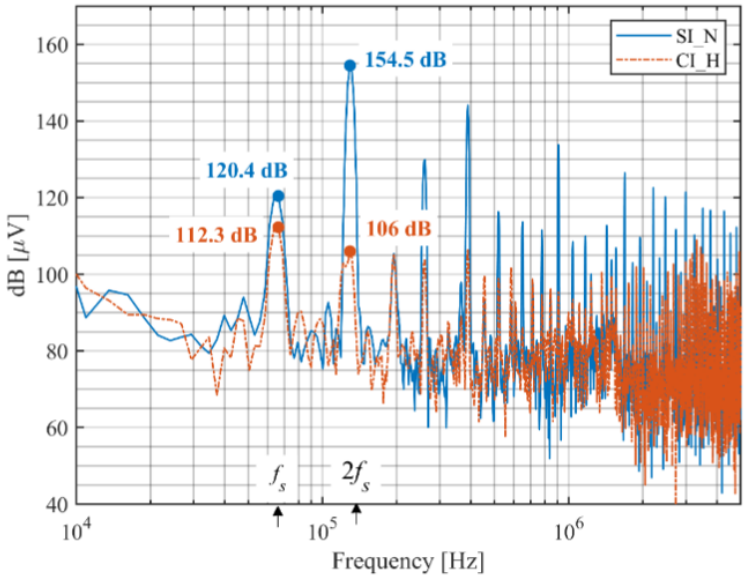

Fig. 19 Common-mode noise comparison for different inductor structures and control methods.

As can be seen in all the presented figures, the new structure can be effectively employed as a worthy counterpart to other state-of-the-art approaches. The proposed alternate common-leg coupled inductor configuration with H-type control shows favorable characteristics, as it allows for a lower number of components than the SI option, decent individual current ripples, and low output current ripples while maintaining a simple magnetic design compared to other coupled-inductor-based options, and vastly reduced CM noise. Thus, the proposed solution of the common-leg coupled inductor applied in a three-level dc-dc converter based on SiC power devices is a noteworthy option for dc-dc power conversion in the medium voltage range, especially for applications concerning battery energy storage, photovoltaics, and EV charging stations.

8. Summary

The developed DC/DC battery converter to be applied in the MoReSiC system was successfully proposed and validated, both in simulations and through experimental tests using two different experimental models. The converter with the applied control method fulfills all the requirements; the converter reaches the set reference values using both voltage and current control, as well as is capable of balancing the DC-link voltages when needed while maintaining levelled inductor currents. Furthermore, the full experimental study regarding the required operation, including tests rated at 20 kW in both directions, is provided. Therefore, both deliverables D.5.1 and D.5.2 have been reached, as well as the milestone. Moreover, additional tests exhibiting novel common-leg coupled inductor structure have also been performed. All in all, the WP has been finalized.

.